ChemPubSoc Europe

DOI: 10.1002/ejic.201901173

EurJIC European Journal of Inorganic Chemistry

Full Paper

Unsymmetric Diiron Complexes

Structural Differences and Redox Properties of Unsymmetric Diiron PDIxCy Complexes

Andreas J. Hofmann,[a] Christian Jandl,[a] and Corinna R. Hess*[a]

Abstract: We present two bimetallic iron complexes, $[Fe_2(PDIeCy)(OTf)_4]$ (**1**) and $[Fe_2(PDIpCy)(THF)(OTf)_4]$ (**2**) coordinated by an unsymmetric ligand. The new ligand, PDIeCy (PDI = pyridyldiimine; e = ethyl; Cy = cyclam), is a variant of the previously reported PDIpCy (p = propyl) ligand, featuring a shorter linker between the two metal coordination sites. The structural and electronic properties of **1** and **2**, both in the solid and solution state, were analyzed by means of X-ray crystallography, and spectroscopic methods, including ^{19}F-NMR. The two ligand platforms yield markedly different diiron structures: the PDIeCy ligand permits formation of a bridged, μ-OTf complex, while the two iron centers of the PDIpCy-based **2** remain unconnected, directly, under all conditions examined. Both compounds contain electronically non-coupled high-spin ($S = 2$) ferrous centers, as established by Mössbauer spectroscopy and magnetic susceptibility studies. Cyclic voltammetry demonstrates the rich redox chemistry of the compounds, involving both ligand and metal-centered redox processes. Moreover, we synthesized the two-electron reduced $[Fe_2(PDIeCy)]^{2+}$ form of **1**, which contains the dianionic PDI^{2-} ligand, and represents a two-electron charge localized complex.

Introduction

Binuclear iron sites are employed by enzymes for varied biological processes that entail dioxygen activation (hemerythrin, MMO, RNRs), NO reduction (FNORs), and H_2 chemistry, and feature in the active sites of hydrolases (PAPs, GliJ).[1–10] The combination of two redox-active iron centers in close proximity confers advantages for catalysis, including cooperative binding and activation of substrates, and the use of both metal ions for multi-electron processes. Many biomimetic diiron complexes have been generated as spectroscopic and mechanistic probes for the enzymes, and as synthetic catalysts for related chemistry.[10–19] A notable feature among several of the aforementioned enzyme active sites is the asymmetric coordination environment. Differing ligand environments, correlated with distinct electronic properties, allow each metal center to adopt a unique role in the overall reaction.[19,20] Accordingly, a number of bio-inspired, unsymmetric complexes — not only of iron, but with other metals — have been reported in recent years, which merge unique coordination environments.[21–28]

We recently developed the unsymmetric PDIpCy ligand, which combines a pyridine diimine (PDI) and a cyclam (Cy) group, to support dinuclear complexes thereof (Scheme 1).[29] We reported the synthesis of non-coupled homo- and heterobimetallic Ni- and Zn-containing PDIpCy complexes. We now have focused our attention on diiron compounds. Iron offers

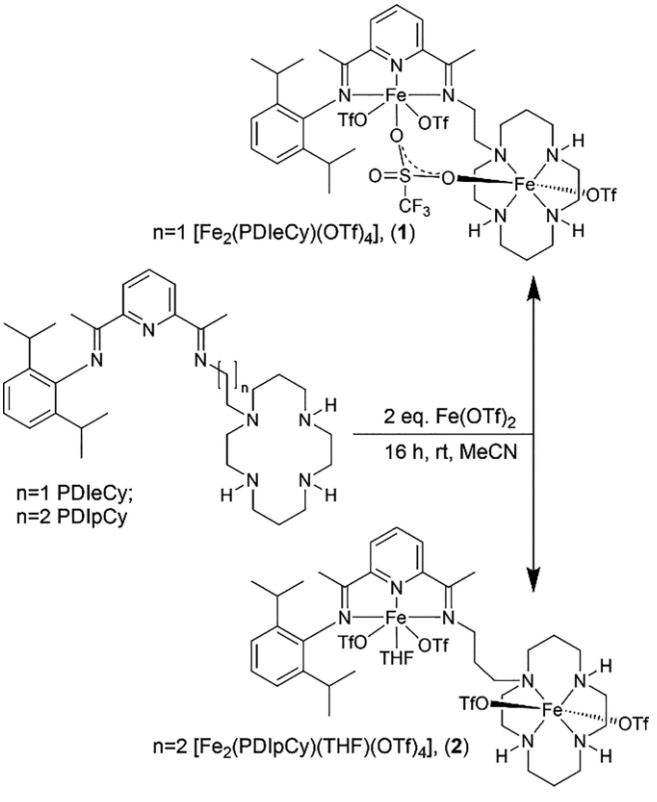

Scheme 1. Synthesis of **1** and **2**.

[a] *Department of Chemistry and Catalysis Research Center, Technische Universität München, Lichtenbergstraße 4, Garching 85748, Germany*
E-mail: corinna.hess@ch.tum.de
https://www.department.ch.tum.de/bioinorganic/home/

Supporting information and ORCID(s) from the author(s) for this article are available on the WWW under https://doi.org/10.1002/ejic.201901173.

access to a wider range of oxidation states, and Fe-PDI and -cyclam complexes are uniquely suited for a variety of redox and organometallic reactions, including several of the aforementioned biologically relevant reactions.[30–46] We envisioned that the combined scope of reactions facilitated by the two types of Fe compounds might give rise to unique activities.

Furthermore, we have generated a variant of the previously reported PDIpCy ligand, PDIeCy, in which the propyl-linker of the molecule is replaced by a shorter ethyl group. We expected that the PDIeCy might allow a closer approach of the two metal centers. In this work, we describe our initial studies to characterize the two diiron complexes, using X-ray crystallography, spectroscopic methods and cyclic voltammetry. The structural properties and metal···metal interactions of the Fe_2-PDIpCy and -PDIeCy were compared, as these features are relevant to potential cooperative reactivity within these systems. Examination of the redox properties provides insight into the electron donor and acceptor capacity of the combined PDI/Cy system.

Results and Discussion

Synthesis and Solid State Characterization

PDIeCy was generated according to a similar procedure as reported for the synthesis of PDIpCy, involving the reaction of 2,6-diacetylpyridine with 2,6-diisopropylaniline and 1-(2-aminoethyl)-1,4,8,11-tetraazacyclotetradecane, respectively (Scheme S1). The diiron complexes of the two ligand scaffolds, $[Fe_2(PDIeCy)(OTf)_4]$ (**1**; OTf = trifluoromethansulfonate) and $[Fe_2(PDIpCy)(THF)(OTf)_4]$ (**2**), were synthesized upon addition of two equiv. of $Fe(OTf)_2$ to the respective ligand in MeCN at room temperature (Scheme 1). The composition of the bimetallic complexes was verified by mass spectrometry and elemental analysis.

Single crystals of both **1** and **2** were successfully obtained from a tetrahydrofuran (THF)/pentane solution (CCDC 1912170, CCDC 1912171). Although the crystalline sample of **2** was significantly twinned, we were able to solve the crystal structure and to model the (disordered) molecular structure of the dinuclear complex. We therefore refrain from a detailed discussion of geometrical parameters and use this data only as structural proof. The structure of **2** (Figure 1) resembles the previously reported complexes $[Zn_2(PDIpCy)(THF)(OTf)_4]$ and $[NiZn(PDIpCy)(THF)(OTf)_4]$. The metal centers of **2** are separated by roughly 8 Å, and each iron adopts a pseudo-octahedral geometry. The Fe residing in the PDI unit is additionally ligated by two κ*O*-triflate ligands (Fe_{PDI}–O_{avg} = 2.14 Å) and a THF molecule. The Fe_{Cy} coordination sphere also is completed by two κ*O*-triflate ligands (Fe_{Cy}–O_{avg} = 2.26 Å) arranged *trans* to each other. The shorter linker of the PDIeCy results in significant changes to the binuclear structure. The Fe centers of **1** are bridged by a μ-triflate molecule that coordinates via one O-atom to each metal ion. Consequently, the Fe···Fe distance in **1** is reduced to 5.6 Å (Figure 1). Each iron center of **1** again adopts a six-coordinate geometry, with additional terminal triflate ligands in the remaining coordination positions. Overall, the Fe1–O bond lengths are shorter than the Fe2–O distances (Fe1···O_{avg} = 2.11 Å; Fe2···O_{avg} = 2.31 Å). This trend was observed for PDIpCy complexes containing other metals and for **2**.[29] The bridging triflate thus binds in an asymmetric fashion in **1**, closer to the PDI site.

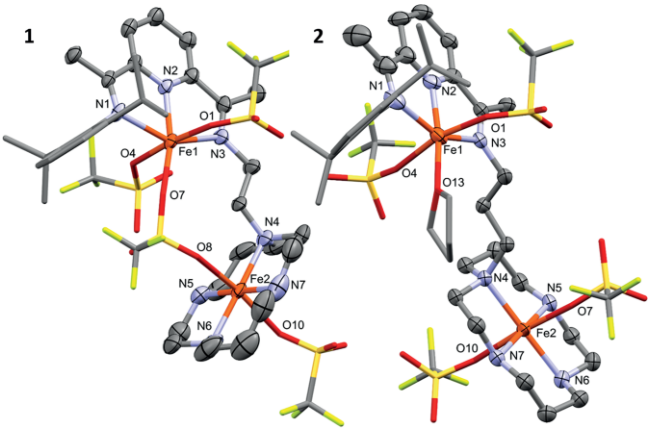

Figure 1. Molecular structure of **1** (left) and **2** (right) in the solid state (50 % probability ellipsoids). Hydrogen atoms, solvent molecules and partial disorder are omitted for clarity.

The structural differences between **1** and **2** influence the packing features in the solid state. The N–H groups of the cyclam moiety in **1** only form intramolecular hydrogen bonds with coordinated triflate anions on both Fe atoms (Figure S32). In contrast, the crystal structure of **2** shows intermolecular hydrogen bonds between the cyclam N-Hs and triflates of adjacent complexes, or co-crystallized THF, leading to chain formation (Figure S33).

Electronic Structure

Mössbauer spectroscopy and magnetic susceptibility studies were carried out on solid samples of **1** and **2** to examine the electronic structures of the diiron complexes, and to determine whether differences in the structure influence the M···M interactions. Figure 2 shows the Mössbauer data of **1**; a two-

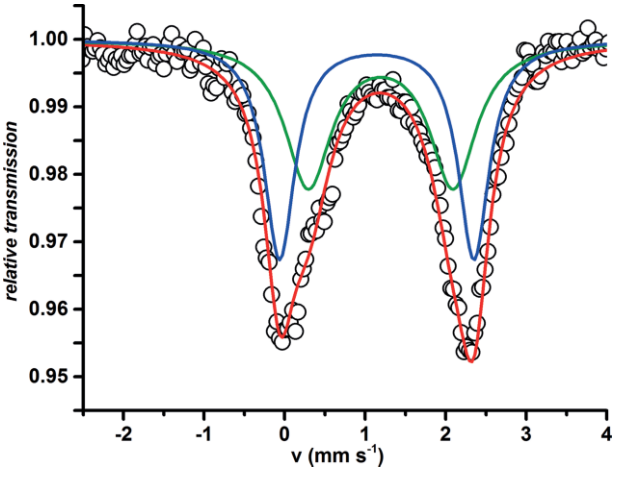

Figure 2. Mössbauer spectrum (80 K) of **1**. Experimental data shown as black circles. The red line represents the combined fit of the individual fits for each Fe center; green line affords $\delta(|\Delta E_Q|)$: 1.19 (1.80) mm s^{-1}, blue line affords $\delta(|\Delta E_Q|)$: 1.14 (2.41) mm s^{-1}.

component fit reveals comparable parameters for the two iron sites, with $\delta(|\Delta E_Q|)$: 1.19 (1.80) mm s^{-1} and $\delta(|\Delta E_Q|)$: 1.14 (2.41) mm s^{-1}. Similar values were obtained for **2** ($\delta(|\Delta E_Q|)$: 1.21 (2.48) mm s^{-1} and $\delta(|\Delta E_Q|)$: 1.06 (2.55) mm s^{-1}; Figure S6), demonstrating that the triflate bridge does not significantly affect the individual Fe^{II} centers. The Mössbauer data clearly denote the presence of two high-spin, $S = 2$, ferrous ions in each complex.

Magnetic susceptibility measurements verified the spin state of the complexes (Figure 3 and Figure S7). The effective magnetic moment of **1** remains constant at 7.3 μ_B between 300 K and 70 K and decreases to a final value of 4.1 μ_B at 2 K. The room temperature magnetic moment is close to the spin-only value for two non-coupled high-spin iron(II) ions (6.9 μ_B), and well below that for a strongly coupled $S = 4$ system (8.9 μ_B). The data were fit according to the spin Hamiltonian, including exchange coupling and zero-field splitting terms (see SI for details, and Figure S8),with two $S = 2$ centers. The best fit was obtained with $g = 2.1$, $J = 0.01$ cm^{-1}, $|D| = 17.5$ cm^{-1}, and $E/D = 0.32$. The negligible exchange coupling constant demonstrates that the two iron centers in **1** are non-coupled, despite the bridging triflate. Similar *J*-values were reported for other μ-triflate diiron complexes.[47–49] The magnetic susceptibility data for **2** gave similar values, where the best fit was obtained with $g = 2.17$, $J = 0.07$ cm^{-1}, $|D| = 17.7$ cm^{-1}, and $E/D = 0.33$ (Figures S7 and S9).

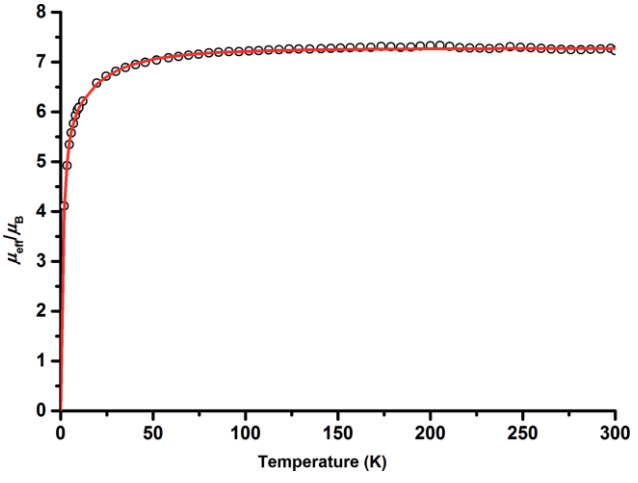

Figure 3. Magnetic susceptibility data for **1** (2–300 K). Circles represent the experimental data; red line represents the simulation, which affords: $S_1 = S_2 = 2$, $g_1 = g_2 = 2.10$, $J = 0.01$ cm^{-1}, $|D_1| = |D_2| = 17.5$ cm^{-1}, $E/D_1 = E/D_2 = 0.26$, TIP = 2.39×10^{-3} emu.

Solution State Characterization

While the minor modification to the ligand backbone leads to differences in the molecular structures of **1** and **2**, we questioned whether the coordination of the triflate molecules persists in solution. The solution state behavior of the bimetallic complexes is relevant to their potential use as homogeneous catalysts. To support the solution state characterization of **1** and **2**, a related complex, $[Fe_2(PDIeCy)(MeCN)_3](PF_6)_4$ (**3**), was synthesized upon reaction of PDIeCy with two equivalents of $[Fe(MeCN)_6](PF_6)_2$. Compound **3** includes the PDIeCy backbone, and otherwise, only MeCN molecules that can complete the iron coordination sphere but are unlikely to bridge the two iron centers. The complex thus acts as a benchmark for evaluation of the spectroscopic and redox properties of the triflate-based analogues.

The absorption spectra of **1** and **2** in the non-coordinating solvent DCM (Figure S10) are dominated by transitions of the PDI site. The absorptions in the UV region ($\lambda_{max} = 300$ nm) are due to π–π* transitions, while the broad band in the visible region (400–700 nm) is assigned to PDI-based MLCT transitions.[50,51] The solid state spectrum of **1** (Figure S11) closely resembles the solution state spectrum. However, the spectrum of **3** in DCM is noticeably different, lacking features from 550–700 nm (Figure S12).

To further probe the coordination chemistry of the triflate ligands, ^{19}F-NMR were obtained for **1** and **2**. The ^{19}F-NMR spectrum of **1** in DCM (Figure S13) at 20 °C exhibits seven signals that appear between 75 and –57 ppm. These signals divide upon cooling of the sample, which may be due to greater asymmetry or slower ligand exchange at low temperature. As the resonances of bridging triflates are shifted downfield with respect to those of terminally bonded triflates,[52,53] the signal at 75 ppm at 20 °C can be assigned to the former.

The spectra of **2** also exhibit multiple signals (Figure S14), however the resonance at 75 ppm is not observed, indicating that a triflate bridged conformation is absent for the PDIpCy complex. The broad signals at –57 ppm (20 °C) in the spectra of both complexes can be assigned to non-coordinated triflate counterions.[52,54] This suggests multiple conformations are available in which one or both sites may be less than six-coordinate in solution. The various resonances in the NMR spectra could not be precisely assigned. However, the data clearly show differences between the spectra of **1** and **2**, and indicate that the bridged conformation of **1** persists in DCM.

The electronic spectra of all three diiron complexes are virtually identical in MeCN (Figure 4). The bands in the visible region are red-shifted ($\lambda = 410$–570 nm) with respect to their position in the DCM spectra of **1** and **2**. The transitions in the spectrum of **3** have a slightly lower intensity than those of **1** and **2** — which may reflect an additional effect due to the counteranion — however, the overall shape and band positions are the same.

Interestingly, upon cooling, a marked change in the absorption bands of all three diiron complexes is observed (Figure 4, Figure S15 and Figure S16); the transitions in the visible region increase in intensity and become more distinct. The changes in the absorption spectra coincide with an isosbestic point at 371 nm (Figure 4 bottom, inset), indicating clean conversion between two forms of the molecule. The original spectrum also is fully restored upon return of the sample to room temperature, following the variable temperature measurements. We attribute the behavior to changes occurring at the Fe-PDI site, since the spectrum of the monometallic $[(iPrPDI)Fe(OTf)_2]$[55] also increases in intensity upon cooling (Figure S17). However, the changes in the absorption features of the mononuclear complex are less significant than those of the bimetallic compounds, suggesting that the second metal site may play a role

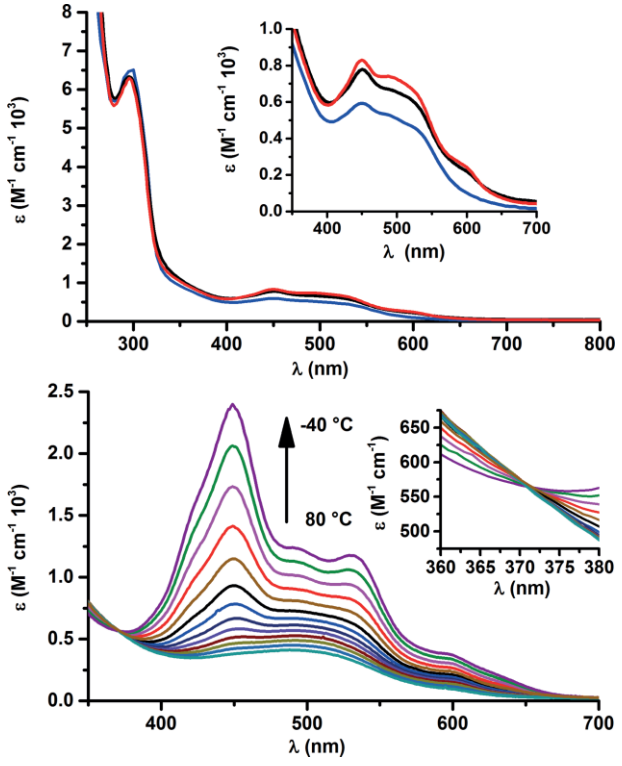

Figure 4. Top: electronic spectra of **1** (black), **2** (red) and **3** (blue) in MeCN at room temperature. Bottom: temperature dependent absorption spectra of **1**.

in this phenomenon. The ^{19}F-NMR spectra for **1** and **2** show only one resonance in the temperature range of –40 °C to +80 °C (Figure S18 and Figure S19). This signal, due to the uncoordinated triflates, shifts moderately from –78.8 ppm to –63.5 ppm with increasing temperature. Thus, the absorption spectra and ^{19}F-NMR data indicate that the triflate ligands of **1** and **2** are readily displaced by acetonitrile, and coordination equilibria involving the triflate ions cannot account for the temperature dependent changes in the absorption spectra. Moreover, the same temperature dependent changes in the absorption spectrum also are observed for **3** (Figure S16), which lacks any triflate ions.

The solution state magnetic susceptibilities of **1** and **2** (MeCN-d_3 or propionitrile; see SI for details) were determined by Evan's method, to probe whether changes in the spin state of the bimetallic complex might occur. The room temperature effective magnetic moments of 7.0 μ_B (**1**) and 7.1 μ_B (**2**) determined by NMR are comparable to the values obtained from the solid-state SQUID data. The data confirm that both iron centers remain high-spin in solution, even upon coordination of acetonitrile. The magnetic moments remain fairly constant from 90 to –20 °C, but decrease at lower temperatures yielding final values of 5.8 μ_B (**1**) and 5.7 μ_B (**2**) at –90 °C (Table S1; Figures S20 – S22). Since the absorption bands of **1** and **2** continue to decrease in intensity above –20 °C, spin state changes do not appear to fully account for the absorption spectral changes. Although we have not identified the origin of the spectral changes, differences in the coordination number (and thus geometry) at the Fe-PDI site,[56] or in the electronic structure (e.g. valence tautomerism between the Fe center and the redox-active PDI) offer possible explanations.

Redox Properties

Cyclic voltammetry was carried out to examine the redox properties of the bimetallic complexes. The CV of **1** shows five redox couples in the range of –1.7 to 1.2 V vs. $Fc^{+/0}$ (Figure 5; Table 1). Two reductions occur at –1.2 and –1.6 V. The potentials are similar to the values observed in the CV of $[Zn_2(PDIpCy)(OTf)_4]$,[29] and are likewise assigned to the $PDI^{0/-}$ and $PDI^{-/2-}$ couples of the diiron complex. The assignment is in accord with the redox behavior established for other Fe-PDI complexes, in which ligand-centered reduction occurs prior to metal-centered reduction.[57,58] The CV of **1** additionally exhibits a series of seemingly reversible oxidative couples that were resolved using differential pulse voltammetry (DPV; Figure 5). The oxidative processes consist of two closely spaced events at 0.4 and 0.6 V, followed by a third oxidation at 1.0 V. The first two couples are tentatively assigned to the oxidation of the two divalent Fe centers to their ferric forms. The final oxidative event would then correspond to formation of an Fe^{IV} species. Fe^{IV}-cyclam species are well-established,[59] and the $Fe^{IV/III}$ couple of

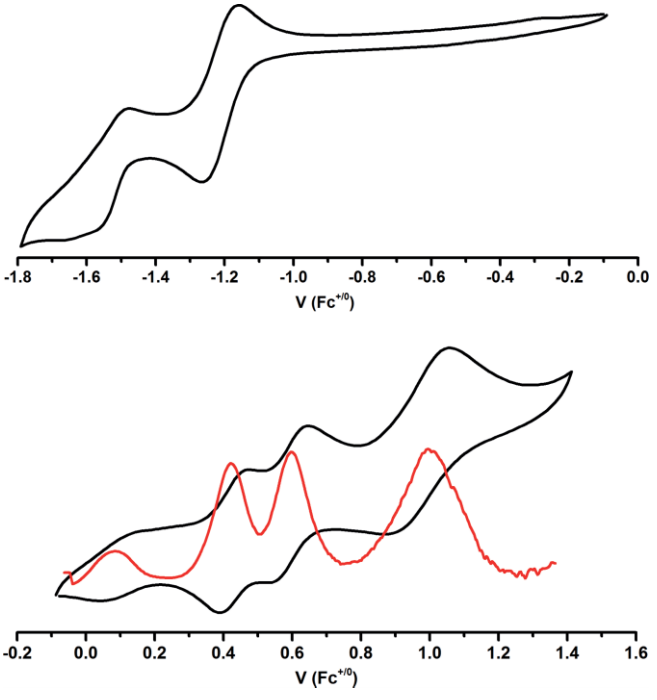

Figure 5. Top: CV of **1** (MeCN, 0.1 M $[N(nBu)_4]PF_6$, 0.1 V s^{-1}) in the reductive region. Bottom: differential pulse voltammetry (DPV) and cyclic voltammetry (CV) of **1** (MeCN, 0.1 M $[N(nBu)_4]PF_6$, 20 mV s^{-1}) showing the oxidative events.

Table 1. Electrochemical data for **1–3** (MeCN, 0.1 M $[N(nBu)_4]PF_6$, 0.1 V s^{-1}).

Redox process	$E_{1/2}$, V vs. $Fc^{+/0}$		
	1	**2**	**3**
PDI^0/PDI^-	–1.5	–1.6	–1.5
PDI^-/PDI^{2-}	–1.2	–1.2	–1.2
$Fe^{III/II}_{PDI}$ & $Fe^{III/II}_{Cy}$	0.4, 0.6	0.4, 0.5	0.5

an iron cyclam complex at 1.15 V was reported by Wieghardt et al.[60] Thus, the assignment is not without precedent, but further studies are warranted to verify the nature of the oxidative processes.

All five redox events of **2** and **3** occur at similar potentials (Table 1, Figure S23–S26). The slight changes in the ligand backbone do not have an effect on the redox processes that occur at the individual metal sites. Overall, the diiron complexes exhibit a rich and unique redox chemistry. Reduction of the complexes is ligand-centered and occurs exclusively at the PDI unit of the complex, whereas the oxidative processes are metal-centered and may involve both sites.

Reduced Complexes

To confirm our assignments of the reductive events, we chemically generated the one- and two-electron reduced forms of **1**. We have focused our current studies on the reduced forms of the complexes, since we were interested in determining whether a two-electron charge-localized complex — *formally* a two-electron mixed valence complex — could be stably generated, as implied by the CV data. The addition of one or two equivalents of $CoCp^*_2$ to a solution of **1** in THF leads to formation of $[Fe_2(PDIeCy)(THF)(OTf)_3]$ (**4**) and $[Fe_2(PDIeCy)(THF)(OTf)_2]$ (**5**), respectively (compositions as determined by CHN analysis). The solution state effective magnetic moment of **4** (6.5 μ_B) agrees with two uncoupled S = 1.5 and S = 2 sites (spin only value = 6.2 μ_B). Likewise, the presence of two non-coupled S = 1 and S = 2 sites in **5** are supported by the magnetic susceptibility values for this complex (μ_{eff} = 6.0 μ_B; spin-only value = 5.6 μ_B).

IR and absorption spectroscopy indicate that reduction occurs at the PDI site, consistent with our electrochemical assignments. The diimine C-N stretch associated with the PDI unit, as observed in the IR spectrum of **1**, is no longer prominent in the spectra of **4** and **5** (Figure S27). The absorption spectra of the reduced forms also differ from that of **1**. In THF, the spectrum of **1** exhibits a broad absorbance spanning 400–650 nm (λ_{max} = 550 nm), similar to its spectrum in DCM (Figure 6, black trace). The absorption spectrum of **4** (Figure 6, red trace) shows a slight red shift of the bands in the visible region (Figure S28). The changes in the spectrum of the two-electron reduced **5** (Figure 6, blue trace and Figures S29) are more significant, with the appearance of two prominent bands at 345 and 444 nm. Complex **5** additionally features broad transitions in the NIR region. The spectrum of **5** is analogous to that of [(*i*PrPDI)Fe$(N_2)_2$] — containing the PDI^{2-} — reported by Bart et al.[61] The features of the spectra of the two-electron reduced form of **1**, as generated electrochemically (Figure S31), are consistent with those of the chemically generated **5**.

To further confirm that both reductions occur at the PDI-site, we generated the one- and two-electron reduced forms of the monometallic, symmetric [(*i*PrPDI)Fe$(OTf)_2$]. The spectra of its reduced forms (Figure S30) are highly similar to those of **4** and **5**. Minimal changes are likewise observed upon reaction of [(*i*PrPDI)Fe$(OTf)_2$] with one equivalent of $CoCp^*_2$, whereas the two-electron reduced complex also exhibits the distinctive bands in the visible region.

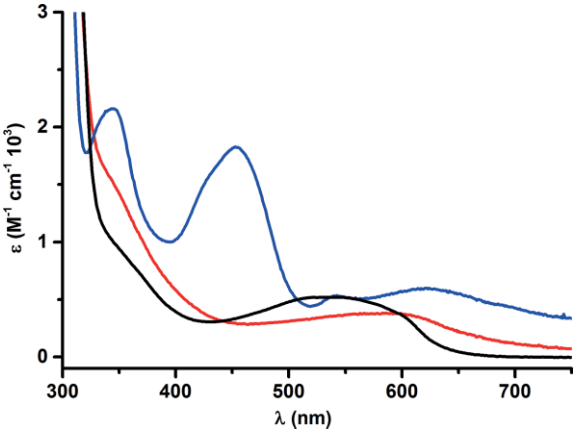

Figure 6. Electronic spectra of **1** (black), **4** (red) and **5** (blue) in THF.

Overall, the data denote that both **4** and **5** are indeed charge-localized complexes. In the latter complex, a formal "$Fe_{PDI}{}^{0}$" site exists alongside an $Fe_{Cy}{}^{II}$ center within the PDIeCy complex; electron transfer between the two metal centers does not seem to take place.

Conclusions

We present two new unsymmetric binuclear iron complexes, wherein the individual coordination environments confer unique properties to each site. Both PDIpCy and PDIeCy scaffolds support high-spin ferrous centers, which are electronically uncoupled. However, the small modification to the PDIpCy backbone — in which the propyl linker is displaced by an ethyl unit — leads to a significant structural change. In the Fe_2-PDIeCy complex, the two Fe ions are bridged by a triflate molecule. In contrast, the slightly larger distance between the PDI and Cy units in PDIpCy ligand does not favor the bridged conformation. The μ-OTf structure of **1**, which persists in non-coordinating solvents as verified by ^{19}F-NMR, clearly demonstrates the potential for cooperative substrate interactions in this compound. Both diiron complexes can access a wide range of redox states, minimally from $[Fe_2(PDIxCy)]^{2+} \rightarrow [Fe_2(PDIxCy)]^{6+}$ (x = ethyl or propyl). The reductive processes are localized at the Fe_{PDI} site as shown by compounds **4** and **5**. Therefore, reduction of the diiron complexes results in the formation of one- and two-electron charge localized forms. The potential to access Fe^{IV}-containing forms of **1** and **2**, as is common for Fe-cyclam complexes, offers advantages for oxidation chemistry.[1,45] The unique properties of the diiron complexes bode promise for their reactivity toward a range of multi-electron processes, and these aspects are currently being explored in ongoing studies in our lab.

Experimental Section

General Procedures: $Fe(OTf)_2$ was purchased from TCI Deutschland GmbH, all other chemicals were purchased from Sigma Aldrich and used as received. Metal complexes were synthesized under inert atmosphere (Ar) using standard Schlenk or glovebox techniques and using anhydrous solvents. Solvents were dried by passage over

activated alumina columns and stored over 3 Å (MeCN, DCM) or 4 Å molecular sieves. MeOH was purchased from Sigma Aldrich and stored over 3 Å molecular sieves. 1-(6-(1-((2,6-diisopropylphenyl)-imino) ethyl)pyridin2-yl)ethan-1-one,[62] N-(3-(1,4,8,11-tetraazacyclotetradecan-1-yl)propyl)-1-(6-(1-((2,6-diisopropylphenyl)-imino)-ethyl)pyridin-2-yl)ethan-1-imine (PDIpCy),[29] 1,4,8-tris(*tert*-butoxycarbonyl)-1,4,8,11-tetraazacyclotetradecane,[63] {2,6- 1-(2-aminoethyl)-1,4,8,11-tetraazacyclotetradecane,[64] and [(*i*PrPDI)Fe(OTf)$_2$][55] were prepared according to literature procedures. Products were verified by NMR spectroscopy and mass spectrometry.

N-(2-(1,4,8,11-Tetraazacyclotetradecan-1-yl)ethyl)-1-(6-((E)-1-((2,6-diisopropylphenyl)-imino)ethyl)pyridin-2-yl)ethan-1-imine (PDIeCy): 1-(2-aminoethyl)-1,4,8,11-tetraazacyclo-tetradecane (1.15 g, 4.7 mmol, 1 equiv.) was dissolved in 20 mL of anhydrous MeOH and 1-(6-(1-((2,6-diisopropylphenyl)imino)-ethyl)pyridin2-yl)ethan-1-one (1.50 g, 4.7 mmol, 1 equiv.) was added. The mixture was heated to 60 °C for 40 h, cooled with an acetone/liquid nitrogen bath to –78 °C and filtered. The filtrate was concentrated under vacuum. The resultant yellow oil was dissolved in dry MeCN and filtered through Celite. Upon cooling of the solution to –40 °C, the product was obtained as a yellow solid that was filtered from the solution (978 mg, 1.79 mmol, 38 %). ^{1}H NMR (400 MHz, $CDCl_3$) δ = 8.34 (d, J = 7.7 Hz, 1H), 8.17 (d, J = 7.9 Hz, 1H), 7.79 (t, J = 7.8 Hz, 1H), 7.15 (d, J = 7.5 Hz, 2H), 7.08 (dd, J = 8.5, 6.5 Hz, 1H), 3.71 (t, J = 7.2 Hz, 2H), 3.04–2.53 (m, 23H), 2.44 (s, 3H), 2.23 (s, 3H), 1.85–1.78 (m, 2H), 1.75–1.74 (m, 2H), 1.14 (d, J = 6.9, 12H). ^{13}C (100 MHz, DCM-d_2) 167.12, 166.74, 156.81, 154.99, 146.77, 136.75, 135.97, 123.65, 123.12, 122.02, 121.50, 55.68, 53.41, 53.37, 50.83, 50.02, 49.27, 49.09, 48.95, 48.28, 48.06, 29.22, 28.47, 26.89, 23.35, 22.97, 17.23, 14.03. MS (LIFDI): m/z (%): 548.4 [M + (H$^+$)]$^+$.

[Fe$_2$(PDIeCy)(OTf)$_4$] (1): PDIeCy (50 mg, 91 µmol, 1 equiv.) and Fe(OTf)$_2$ (65 mg, 182 µmol, 2 equiv.) were dissolved in 10 mL of MeCN and the reaction mixture was stirred for 16 h at room temperature. The solvent was removed under vacuum, the residue was dissolved in THF and filtered through Celite. Red crystals of **1** were obtained by slow diffusion of pentane into a solution of the crude product in THF (83 mg, 66 µmol, 72 %). UV/Vis (DCM): $\lambda_{max}(\varepsilon)$ = 550 (630), 332sh (1240), 298 nm (6210 mol^{-1} dm^{3}cm^{-1}); MS (LIFDI): m/z (%): 1107.6 [M–(OTf$^-$)]$^+$; elemental analysis calcd. (%) for $C_{37}H_{53}F_{12}Fe_2N_7O_{12}S_4$: C, 35.39; H, 4.25; N, 7.81; S, 10.21; found C, 35.51; H, 4.34; N, 7.66; S, 10.09.

[Fe$_2$(PDIpCy)(THF)(OTf)$_4$] (2): PDIpCy (70 mg, 125 µmol, 1 equiv.) and Fe(OTf)$_2$ (89 mg, 249 µmol, 2 equiv.) were dissolved in 10 mL of MeCN and the reaction mixture was stirred for 16 h at room temperature. The solvent was removed under vacuum and the residue was dissolved in THF and filtered through Celite. The complex was recrystallized from a THF/pentane solution, yielding **2** as a red crystalline solid (80 mg, 63 µmol, 50 %). Crystals suitable for X-ray diffraction were obtained by slow diffusion of pentane into a solution of the crude product in THF. UV/Vis (DCM): λ_{max} (ε) = 550 (680), 332sh (1320), 298 nm (6290 mol^{-1} dm^{3}cm^{-1}); MS (LIFDI): m/z (%): 1121.3 [M–(OTf$^-$ + THF)]$^+$; elemental analysis calcd. (%) for $C_{38}H_{55}F_{12}Fe_2N_7O_{12}S_4$: C, 35.94; H, 4.37; N, 7.72, S, 10.10; found C, 35.79; H, 4.33; N, 7.78 S, 9.85; (CHN-analysis corresponds to the complex lacking the coordinated THF).

[Fe$_2$(PDIeCy)(MeCN)$_3$](PF$_6$)$_4$ (3): PDIeCy (21.8 mg, 40 µmol, 1 equiv.) and [Fe(MeCN)$_6$](PF$_6$)$_2$ (47.1 mg, 80 µmol, 2 equiv.) were dissolved in 5 mL of MeCN and the reaction mixture was stirred for 4 h at room temperature. The solvent was removed under vacuum, and the residue was washed twice with 2 mL DCM to give **3** as a red powder (61.1 mg, 35 µmol, 89 %). UV/Vis (DCM): λ_{max} (ε) = 477 (390), 342sh (1330), 302 nm (6260 mol^{-1} dm^{3}cm^{-1}); elemental analysis calcd. (%) for $C_{39}H_{62}F_{24}Fe_2N_{10}P_4$: C, 34.38; H, 4.59; N, 10.28, found: C, 34.29; H, 4.68; N, 10.42.

[Fe$_2$(PDIeCy)(THF)(OTf)$_3$] (4): Complex **1** (28.6 mg, 22.8 µmol, 1 equiv.) was dissolved in THF and the solution was cooled to –40 °C. CoCp*$_2$ (7.5 mg, 22.8 µmol, 1 equiv.) was added to the solution, which was subsequently allowed to reach room temperature while stirring. After 16 h, the mixture was filtered through celite to remove [CoCp*$_2$]OTf. The solution was concentrated to 1 mL. Addition of 10 mL pentane to the solution yielded **4** as a blue solid**.** (12.6 mg, 11 µmol, 47 %). UV/Vis (THF): λ_{max} (ε) = 598br (380), 338sh (1610), 296 nm (13930 mol^{-1} dm^{3}cm^{-1}); elemental analysis calcd. (%) for $C_{40}H_{61}F_9Fe_2N_7O_{10}S_3$: C, 40.76; H, 5.22; N, 8.32 S, 8.16; found C, 40.59; H, 5.40; N, 8.05; S, 8.01.

[Fe$_2$(PDIeCy)(THF)(OTf)$_2$] (5): Complex **1** (25.1 mg, 20.0 µmol, 1 equiv.) was dissolved in THF and cooled to –40 °C. Two equiv. of CoCp*$_2$ (13.1 mg, 40.0 µmol, 2 equiv.) were added to the solution, which was subsequently allowed to reach room temperature while stirring. After 16 h, the mixture was filtered through celite to remove [CoCp*$_2$]OTf. The solution was concentrated to 1 mL. Addition of 10 mL pentane to this solution yielded the green solid **5** (8.2 mg, 7.8 µmol, 39 %). UV/Vis (THF): λ_{max} (ε) = 620br (600), 540 (550), 453 (1850), 345 (2150), 296 nm (14870 mol^{-1} dm^{3}cm^{-1}); elemental analysis calcd. (%) for $C_{39}H_{61}F_6Fe_2N_7O_7S_2$: C, 45.49; H, 5.97; N, 9.52 S, 6.23; found C, 45.58; H, 5.95; N, 9.49; S, 6.05.

CCDC 1912170 (for **1**), and 1912171 (for **2**) contain the supplementary crystallographic data for this paper. These data can be obtained free of charge from The Cambridge Crystallographic Data Centre.

Acknowledgments

A. J. H. thanks the TUM Graduate School for financial support. Our thanks go to Dr. A. Pöthig for help with X-ray crystallography, to Prof. T. Fässler for the use of his SQUID magnetometer, M. Boyko for technical assistance with SQUID measurements, and M. Matthews for technical assistance with ^{19}F-NMR spectroscopy. We gratefully acknowledge Dr. E. Bill (MPI for Chemical Energy Conversion) for the Mössbauer spectroscopy measurements and for helpful discussions.

Keywords: Iron · Bimetallic complexes · Redox-active ligands · Ligand effects · Electronic structure

[1] R. Banerjee, J. C. Jones, J. D. Lipscomb, *Annu. Rev. Biochem.* **2019**, *88*, 13.1–13.23.
[2] A. Trehoux, J.-P. Mahy, F. Avenier, *Coord. Chem. Rev.* **2016**, *322*, 142–158.
[3] R. E. Stenkamp, *Chem. Rev.* **1994**, *94*, 715–726.
[4] G. Schenk, N. Mitić, G. R. Hanson, P. Comba, *Coord. Chem. Rev.* **2013**, *257*, 473–482.
[5] G. Schenk, N. Mitić, L. R. Gahan, D. L. Ollis, R. P. McGeary, L. W. Guddat, *Acc. Chem. Res.* **2012**, *45*, 1593–1603.
[6] J. D. M. Kurtz, *Dalton Trans.* **2007**, 4115–4121.
[7] A. Marion, M. Groll, D. H. Scharf, K. Scherlach, M. Glaser, H. Sievers, M. Schuster, C. Hertweck, A. A. Brakhage, I. Antes, E. M. Huber, *ACS Chem. Biol.* **2017**, *12*, 1874–1882.
[8] S. Khatua, A. Majumdar, *J. Inorg. Biochem.* **2015**, *142*, 145–153.
[9] C. Krebs, J. M. Bollinger, S. J. Booker, *Curr. Opin. Chem. Biol.* **2011**, *15*, 291–303.
[10] W. Lubitz, H. Ogata, O. Rüdiger, E. Reijerse, *Chem. Rev.* **2014**, *114*, 4081–4148.
[11] C. J. White, A. L. Speelman, C. Kupper, S. Demeshko, F. Meyer, J. P. Shanahan, E. E. Alp, M. Hu, J. Zhao, N. Lehnert, *J. Am. Chem. Soc.* **2018**, *140*, 2562–2574.

[12] M. Jana, N. Pal, C. J. White, C. Kupper, F. Meyer, N. Lehnert, A. Majumdar, *J. Am. Chem. Soc.* **2017**, *139*, 14380–14383.
[13] T. B. Rauchfuss, *Acc. Chem. Res.* **2015**, *48*, 2107–2116.
[14] T. Glaser, *Coord. Chem. Rev.* **2019**, *380*, 353–377.
[15] S. Friedle, E. Reisner, S. J. Lippard, *Chem. Soc. Rev.* **2010**, *39*, 2768–2779.
[16] P. Comba, L. R. Gahan, G. R. Hanson, V. Mereacre, C. J. Noble, A. K. Powell, I. Prisecaru, G. Schenk, M. Zajaczkowski-Fischer, *Chem. Eur. J.* **2012**, *18*, 1700–1710.
[17] D. M. Heinekey, *J. Organomet. Chem.* **2009**, *694*, 2671–2680.
[18] U. Bossek, H. Hummel, T. Weyhermüller, E. Bili, K. Wieghardt, *Angew. Chem. Int. Ed. Engl.* **1996**, *34*, 2642–2645; *Angew. Chem.* **1996**, *108*, 1653.
[19] A. J. Jasniewski, L. Que, *Chem. Rev.* **2018**, *118*, 2554–2592.
[20] D. A. Whittington, S. J. Lippard, *J. Am. Chem. Soc.* **2001**, *123*, 827–838.
[21] C. Belle, J. L. Pierre, *Eur. J. Inorg. Chem.* **2003**, *2003*, 4137–4146.
[22] C. Incarvito, M. Lam, B. Rhatigan, A. L. Rheingold, C. J. Qin, A. L. Gavrilova, B. Bosnich, *J. Chem. Soc., Dalton* **2001**, 3478–3488.
[23] Y. Sano, N. Lau, A. C. Weitz, J. W. Ziller, M. P. Hendrich, A. S. Borovik, *Inorg. Chem.* **2017**, *56*, 14118–14128.
[24] B. de Souza, G. L. Kreft, T. Bortolotto, H. Terenzi, A. J. Bortoluzzi, E. E. Castellano, R. A. Peralta, J. B. Domingos, A. Neves, *Inorg. Chem.* **2013**, *52*, 3594–3596.
[25] J. L. Wong, R. F. Higgins, I. Bhowmick, D. X. Cao, G. Szigethy, J. W. Ziller, M. P. Shores, A. F. Heyduk, *Chem. Sci.* **2016**, *7*, 1594–1599.
[26] R. J. Eisenhart, L. J. Clouston, C. C. Lu, *Acc. Chem. Res.* **2015**, *48*, 2885–2894.
[27] G. de Ruiter, N. B. Thompson, M. K. Takase, T. Agapie, *J. Am. Chem. Soc.* **2016**, *138*, 1486–1489.
[28] T. Chantarojsiri, J. W. Ziller, J. Y. Yang, *Chem. Sci.* **2018**, *9*, 2567–2574.
[29] R. M. Haas, Z. Hern, S. Sproules, C. R. Hess, *Inorg. Chem.* **2017**, *56*, 14738–14742.
[30] D. Enright, S. Gambarotta, G. P. A. Yap, P. H. M. Budzelaar, *Angew. Chem. Int. Ed.* **2002**, *41*, 3873–3876; *Angew. Chem.* **2002**, *114*, 4029.
[31] Q. Knijnenburg, S. Gambarotta, P. H. M. Budzelaar, *Dalton Trans.* **2006**, 5442–5448.
[32] P. J. Chirik, K. Wieghardt, *Science* **2010**, *327*, 794–795.
[33] M. A. Ortuño, C. J. Cramer, *J. Phys. Chem. A* **2017**, *121*, 5932–5939.
[34] K. T. Sylvester, P. J. Chirik, *J. Am. Chem. Soc.* **2009**, *131*, 8772–8774.
[35] S. M. Rummelt, H. Zhong, I. Korobkov, P. J. Chirik, *J. Am. Chem. Soc.* **2018**, *140*, 11589–11593.
[36] M. Qi, Q. Dong, D. Wang, J. A. Byers, *J. Am. Chem. Soc.* **2018**, *140*, 5686–5690.
[37] G. J. P. Britovsek, V. C. Gibson, S. J. McTavish, G. A. Solan, A. J. P. White, D. J. Williams, G. J. P. Britovsek, B. S. Kimberley, P. J. Maddox, *Chem. Commun.* **1998**, 849–850.
[38] Z. Thammavongsy, T. Seda, L. N. Zakharov, W. Kaminsky, J. D. Gilbertson, *Inorg. Chem.* **2012**, *51*, 9168–9170.
[39] P. M. Cheung, K. T. Burns, Y. M. Kwon, M. Y. Deshaye, K. J. Aguayo, V. F. Oswald, T. Seda, L. N. Zakharov, T. Kowalczyk, J. D. Gilbertson, *J. Am. Chem. Soc.* **2018**, *140*, 17040–17050.
[40] R. P. Yu, J. M. Darmon, J. M. Hoyt, G. W. Margulieux, Z. R. Turner, P. J. Chirik, *ACS Catal.* **2012**, *2*, 1760–1764.
[41] X. Engelmann, D. D. Malik, T. Corona, K. Warm, E. R. Farquhar, M. Swart, W. Nam, K. Ray, *Angew. Chem. Int. Ed.* **2019**, *58*, 4012–4016; *Angew. Chem.* **2019**, *131*, 4052.
[42] A. Annunziata, R. Esposito, G. Gatto, M. E. Cucciolito, A. Tuzi, A. Macchioni, F. Ruffo, *Eur. J. Inorg. Chem.* **2018**, *2018*, 3304–3311.
[43] W. Nam, R. Ho, J. S. Valentine, *J. Am. Chem. Soc.* **1991**, *113*, 7052–7054.
[44] Y. Feng, J. England, L. Que, *ACS Catal.* **2011**, *1*, 1035–1042.
[45] W. Nam, *Acc. Chem. Res.* **2015**, *48*, 2415–2423.
[46] S. P. de Visser, J.-U. Rohde, Y.-M. Lee, J. Cho, W. Nam, *Coord. Chem. Rev.* **2013**, *257*, 381–393.
[47] S. Herold, S. J. Lippard, *J. Am. Chem. Soc.* **1997**, *119*, 145–156.
[48] J. J. Kodanko, S. J. Lippard, *Inorg. Chim. Acta* **2008**, *361*, 894–900.
[49] D. Lee, S. J. Lippard, *Inorg. Chem.* **2002**, *41*, 2704–2719.
[50] I. H. Kuwabara, F. C. M. Comninos, V. L. Pardini, H. Viertler, H. E. Toma, *Electrochim. Acta* **1994**, *39*, 2401–2406.
[51] H. E. Toma, T. E. Chavez-Gil, *Inorg. Chim. Acta* **1997**, *257*, 197–202.
[52] G. J. P. Britovsek, J. England, A. J. P. White, *Inorg. Chem.* **2005**, *44*, 8125–8134.
[53] D. W. Blakesley, S. C. Payne, K. S. Hagen, *Inorg. Chem.* **2000**, *39*, 1979–1989.
[54] H. Börzel, P. Comba, K. S. Hagen, Y. D. Lampeka, A. Lienke, G. Linti, M. Merz, H. Pritzkow, L. V. Tsymbal, *Inorg. Chim. Acta* **2002**, *337*, 407–419.
[55] G. J. P. Britovsek, J. England, S. K. Spitzmesser, A. J. P. White, D. J. Williams, *Dalton Trans.* **2005**, 945–955.
[56] M. Grau, J. England, R. Torres Martin de Rosales, H. S. Rzepa, A. J. P. White, G. J. P. Britovsek, *Inorg. Chem.* **2013**, *52*, 11867–11874.
[57] B. M. Wile, R. J. Trovitch, S. C. Bart, A. M. Tondreau, E. Lobkovsky, C. Milsmann, E. Bill, K. Wieghardt, P. J. Chirik, *Inorg. Chem.* **2009**, *48*, 4190–4200.
[58] S. C. Bart, K. Chłopek, E. Bill, M. W. Bouwkamp, E. Lobkovsky, F. Neese, K. Wieghardt, P. J. Chirik, *J. Am. Chem. Soc.* **2006**, *128*, 13901–13912.
[59] W. Nam, *Acc. Chem. Res.* **2007**, *40*, 522–531.
[60] J. F. Berry, E. Bill, E. Bothe, T. Weyhermüller, K. Wieghardt, *J. Am. Chem. Soc.* **2005**, *127*, 11550–11551.
[61] S. C. Bart, E. Lobkovsky, P. J. Chirik, *J. Am. Chem. Soc.* **2004**, *126*, 13794–13807.
[62] C. Bianchini, G. Mantovani, A. Meli, F. Migliacci, F. Zanobini, F. Laschi, A. Sommazzi, *Eur. J. Inorg. Chem.* **2003**, *2003*, 1620–1631.
[63] L. Fabbrizzi, F. Foti, M. Licchelli, P. M. Maccarini, D. Sacchi, M. Zema, *Chem. Eur. J.* **2002**, *8*, 4965–4972.
[64] Y. H. Lau, J. K. Clegg, J. R. Price, R. B. Macquart, M. H. Todd, P. J. Rutledge, *Chem. Eur. J.* **2018**, *24*, 1573–1585.

Received: October 29, 2019